

CHAPTER 265

Velocity Field Measurements in a "Coastal Buffer Zone"

Hiroshi Yagi¹, Hirofumi Hinata¹ and Kazuo Nadaoka²

Abstract

To investigate the characteristics of flow field in the coastal buffer zone (C.B.Z.), velocity measurements in a field were performed both in non-stratified and stratified conditions. The results of the data analysis have shown that in the non-stratified condition wind action, together with tidal motion, may induce unexpectedly large velocity even near the bottom with the magnitude beyond the threshold of the sediment movement, suggesting that the appreciable sediment transport may be caused by these wind-driven currents in C.B.Z.. In the stratified condition, it is revealed that internal tides with baroclinic velocity fluctuation may dominate the cross-shore exchanging motion of water mass.

INTRODUCTION

In coastal current system, the surf zone and the far-offshore region may be regarded as two extremes in a sense that the former is dominated exclusively by nearshore currents, while the latter is governed mostly by the ocean currents (Fig.1). The intermediate-depth zone, on the other hand, may be affected by both the factors as well as tidal currents, wind-driven currents, density currents, river flow, and hence may be called "coastal buffer zone (C.B.Z.)". Therefore for developing a reliable tool to describe the flow field in this zone, more integrated knowledge on these factors and, if any, the interactions among them are necessary. However, still limited parts

¹ Department of Civil Engineering, Tokyo Institute of Technology, 2-12-1, O-okayama, Meguro-ku, Tokyo 152, Japan.

² Department of Mechanical and Environmental Informatics, Graduate School of Information Science and Engineering, Tokyo Institute of Technology, 2-12-1, O-okayama, Meguro-ku, Tokyo 152, Japan.

of the actual physical process of these factors are known for this purpose (Sato,1995; Yasuda et al.,1995). Hence, in the present study, field measurements in a C.B.Z. have been performed to clarify the fundamental characteristics of its velocity field.

OUTLINE OF FIELD OBSERVATION

The observation was carried out in the Kashima coast, as a typical open coast in Japan, which has a straight sandy beach facing the Pacific Ocean (Fig.2(a)). To clarify the characteristics of the current system in the C.B.Z. both in the non-stratified and stratified conditions, field observations were performed in the periods from Nov. 6 to 28 in 1994 and from July 19 to Aug. 20 in 1995.

In the field measurements, three observation stations (St.1-3) were set to be aligned in the cross-shore direction as shown in Fig.2(b). At these stations electromagnetic current meters, pressure-type wave gauges and thermometer were installed. The location of observation stations and the arrangement of measuring instruments were slightly changed between the observations in the non-stratified and stratified conditions as shown in Fig.2(b).

RESULTS AND DISCUSSTION

Non-stratified condition

Figure 3 shows the time histories, at the three stations, of the mean water surface elevation and the shore-parallel component of the mean velocity close to the bottom (0.7-1.7m above the bottom). These mean values were obtained by a moving time averaging over one hour. The regular diurnal tidal fluctuations appear in the mean surface elevation. On the other hand, the shore-parallel bottom velocity shows appreciable irregularity and its maximum magnitude attains almost 40cm/s at St.1. This is an unexpectedly large value, and such a large near-bottom velocity is observed also by Sato (1995) at the Ishikawa coast facing the Sea of Japan. The velocity of 40cm/s is beyond the threshold for the sediment movement, which is estimated as about 25cm/s by the Shields experimental curve for the sand with the mean diameter of 0.2mm. This fact suggests that in C.B.Z. appreciable sediment transport may be caused by these currents, although conventionally significant sediment transport has been believed to occur mostly in the surf zone and its vicinities.

To find the causes of the large velocities near the bottom, the non-tidal irregular components were extracted from the near bottom velocity data by a moving time average over 24 hours. The results are shown in Fig.4, in which the long-period fluctuations with the period of 6 or 7 days appear at each station. Although the velocity amplitude at St.1 in the shallower region is larger than that at St.3 in the deeper region, their fluctuation patterns are very similar each other. This fact suggests that there exists a common mechanism to cause these long-period velocity fluctuations in the C.B.Z.. To find the mechanism, the wind speed, which is indicated with a thick line in Fig.4 (wind-speed data are partly lacked because of trouble in the measurement), is compared with these long-period velocities.

Obviously there is a close correlation among them. Hence, it is suggested that the wind may induce the long-period fluctuating currents with an appreciable magnitude even near the bottom.

To obtain more quantitative understanding of the wind-driven currents in the C.B.Z., its numerical simulation has been done. The governing equations of the computations are 2-DV momentum equations with the coriolis force and the continuity equation. The k - ε model described below has been employed to evaluate the vertical eddy viscosity ν_t .

$$\frac{\partial k}{\partial t} + u \frac{\partial k}{\partial x} + w \frac{\partial k}{\partial z} = \frac{\partial}{\partial z} \left(\frac{\nu_t}{\sigma_k} \frac{\partial k}{\partial z} \right) + P_k - \varepsilon, \quad (1)$$

$$\frac{\partial \varepsilon}{\partial t} + u \frac{\partial \varepsilon}{\partial x} + w \frac{\partial \varepsilon}{\partial z} = \frac{\partial}{\partial z} \left(\frac{\nu_t}{\sigma_\varepsilon} \frac{\partial \varepsilon}{\partial z} \right) + C_{\varepsilon 1} \frac{\varepsilon}{k} P_k - C_{\varepsilon 2} \frac{\varepsilon^2}{k}, \quad (2)$$

$$\nu_t = C_\mu \frac{k^2}{\varepsilon}, \quad (3)$$

where x and z represent the cross-shore and vertical coordinate, u and w the velocity components in the x - and z -direction, k the kinetic energy of turbulence, ε the dissipation rate of the turbulence kinetic energy, and P_k the production rate of k . C_μ , $C_{\varepsilon 1}$, $C_{\varepsilon 2}$, σ_k and σ_ε are the turbulence model parameters, for which the standard values ($C_\mu=0.09$, $C_{\varepsilon 1}=1.44$, $C_{\varepsilon 2}=1.92$ and $\sigma_k=\sigma_\varepsilon=1.0$) are adopted here. In the present computation, the shore-parallel uniformity is assumed and the topography of the computational area is simplified as shown in Fig.5. The spatially uniform wind shear stress at the water surface was given, being based on the wind data obtained at the nearshore observation station (as shown in Fig.4) and the friction factor at the water surface ($C_d=0.002$).

Figure 6 shows the computed vertical profiles of the shore-parallel velocity for the three cases of the water depth; i.e. $h=20, 60, 100$ m. The indicated results are those after 9.5 days from the beginning of the computation. In the case of $h=100$ m, the vertical gradient is relatively large in the surface layer, while it becomes small beneath it. This fact suggests that the effect of wind shear stress is limited to the surface boundary layer, and the geostrophic current under the balance between the coriolis force and the cross-shore gradient of the water surface elevation is formed beneath the surface layer. On the other hand, in the case of $h=20$ m, the influence of wind shear stress reaches the bottom so that the large vertical gradient of velocity is induced through the entire depth. This means that in the present observation area, because of its shallow water depth less than 20m, the large bottom velocity may be induced by the wind shear stress. These facts indicate that the ratio between the surface Ekman boundary layer width δ_E and the local water depth h , δ_E/h , is one of

the principal factors for the overall understanding of the velocity field of a C.B.Z..

Figure 7 represents the computed time histories of shore-parallel bottom velocities at St.1 to 3, which show the long-period fluctuation similar to those found in Fig.4. However, the magnitude of the computed velocity, except for St.3, is smaller than that of the measured, and the velocity differences among the three stations are not well reproduced. One of the possible causes of these discrepancies is the difference between actual and simulated turbulence structure of the wind-driven currents. Besides the offshore wave breaking due to wind may act to augment the bottom velocity (Yasuda et al., 1995).

Stratified condition

Figure 8 (a) and (b) show respectively the shore-parallel and cross-shore components of the bottom velocity fluctuation in the case of the stratified condition at St.2, where the water depth is 13m and the distance from the shoreline is 1.5km. The long-period fluctuation as found in the non-stratified condition does not appear in this case. However, more conspicuous feature in the time variation characteristics can be found; namely, as compared with those in the non-stratified condition, these velocity data show high frequency fluctuation with appreciable irregularity, especially in the cross-shore component. To examine the frequency characteristics of these velocity fluctuations, the frequency spectra have been computed as shown in Fig.9, which indicate that in the shore-parallel component the diurnal tidal fluctuation has dominant contribution to the spectrum both in the surface and bottom velocities. In the cross-shore velocity component, on the other hand, the diurnal tidal fluctuation prevails in the surface velocity, while in the bottom velocity the semi-diurnal fluctuation arises with appreciable magnitude.

These diurnal and semi-diurnal velocity fluctuations were further examined with the water surface tidal fluctuation by extracting them from the raw data by applying a band-pass filtering. The results are shown in Fig.10 and indicate that the diurnal components of the shore-parallel velocity in the surface and bottom layer are nearly in phase. This means that the shore-parallel velocity is governed mainly by the *barotropic* tidal motion. On the other hand, the semi-diurnal components of the cross-shore velocity in the surface and bottom layer are mutually 180 degrees out of phase. These facts suggest that the *baroclinic* tidal motion is dominant in the cross-shore direction.

To examine the cross-shore barotropic motion in more detail, the water temperature variations both in time and space has been investigated. The field data for this purpose was obtained with the vertical arrays of several thermometers at the three stations. Figure 11 represents a typical example of the time sequence of the spatial distribution of the water temperature. It can be seen that the bottom water body with relatively low temperature runs up and down on the sloping sea bottom with the excursion length of about 1 km for the front movement. Corresponding to this bottom water motion, the upper water body with higher temperature shows cross-shore oscillating motion in the opposite phase from the bottom water motion.

From these results, the velocity field of the C.B.Z. in the stratified condition may

be summarized as follows; i.e., in the shore-parallel direction, the barotropic tidal motion is dominant, while in the cross-shore direction the baroclinic tidal fluctuation is significant. This difference may be explained by the role of the shore boundary; i.e. it prevents the barotropic tidal motion exclusively in the cross-shore direction. However, the baroclinic cross-shore tidal motion appears as running up and down motion near the shore with large excursion length. Since this baroclinic tidal motion results in appreciable cross-shore exchange of water mass, it may have a dominant role in the cross-shore mass transfer in C.B.Z..

CONCLUSIONS

The major conclusions obtained in the present study for C.B.Z. are summarized as follows:

1. In the non-stratified condition, wind action may induce unexpectedly large velocity even near the bottom with the magnitude beyond the threshold of the sediment movement. This fact suggests that the wind-driven current may cause appreciable sediment transport in the C.B.Z..
2. The ratio between the surface Ekman boundary layer width δ_E and the local water depth h is one of the principal factors for overall understanding of the velocity field in C.B.Z..
3. In the stratified condition, internal tide with baroclinic velocity fluctuation may dominate the cross-shore exchanging motion of water mass.

References

- Sato, S. (1995): Characteristics of wave and current induced by low pressures in Japan Sea, *Journal of Hydraulic, Coastal and Environmental Engineering*, JSCE, No.521, 113-122. (*in Japanese*)
- Yasuda, T., Mori, N., Kato, S. and Sato, S. (1995): Currents off the Ishikawa coast and their breaker effects, *Proc. of Coastal Engineering*, JSCE, Vol.42, 431-435. (*in Japanese*)

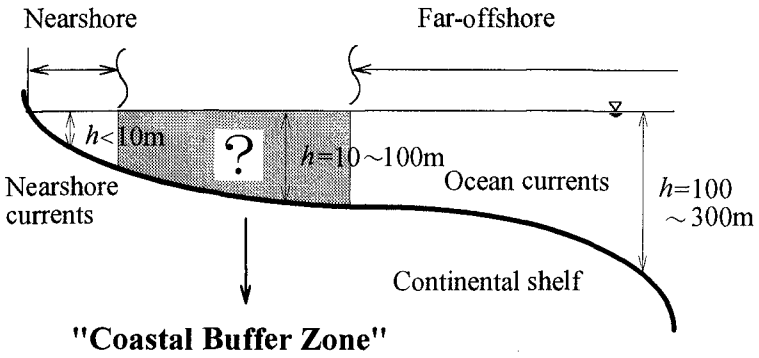


Fig.1 Conceptual illustration of coastal buffer zone in an open coast.

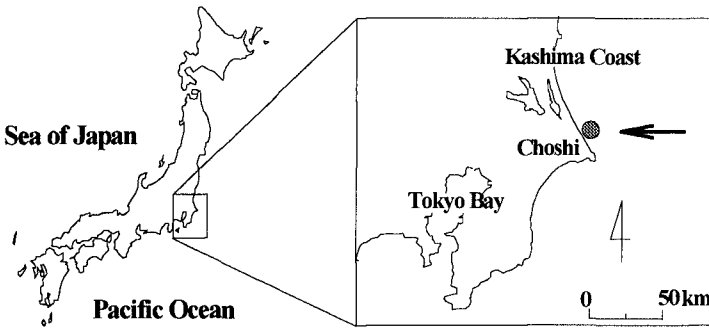


Fig.2(a) Location of study.

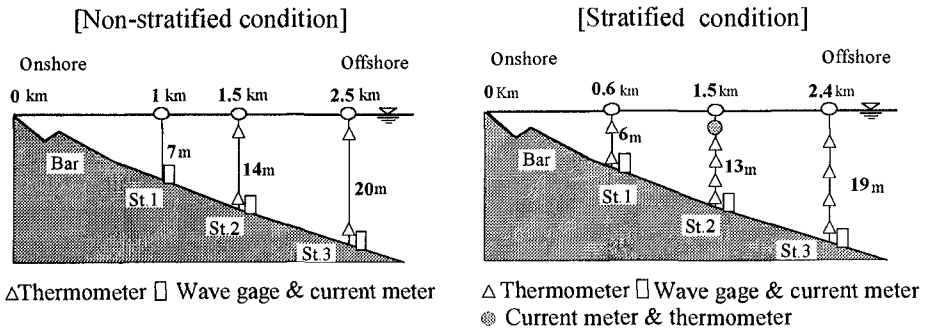


Fig.2(b) Location of observation stations and arrangement of measuring instruments.

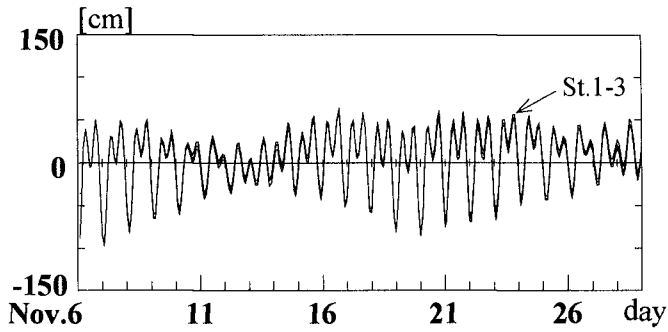


Fig.3 (a) Mean water surface elevations.

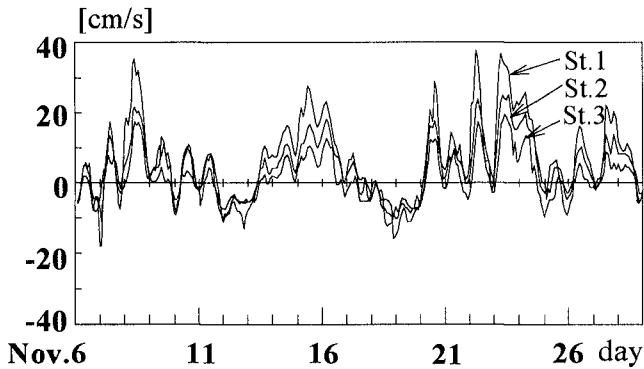


Fig.3 (b) Shore-parallel component of bottom velocities.

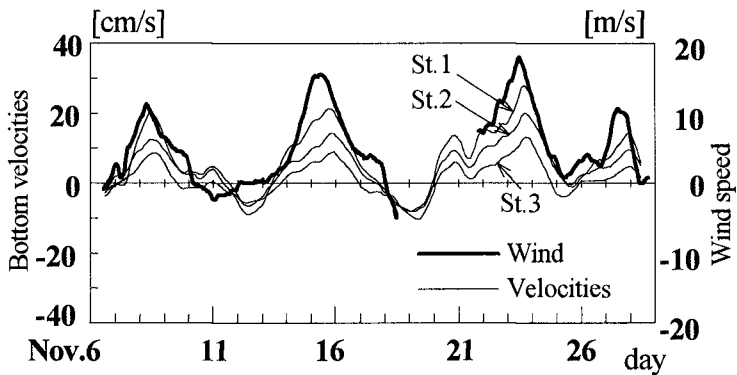


Fig. 4 Long-period fluctuating components of shore-parallel bottom velocities and wind speed.

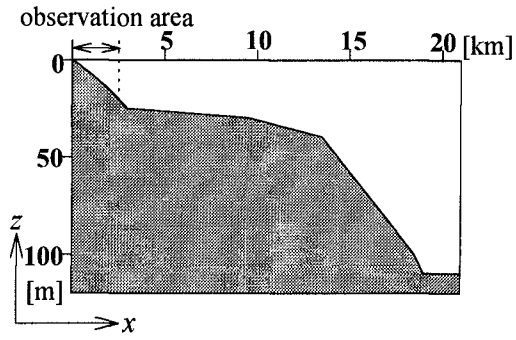


Fig.5 Computational area.

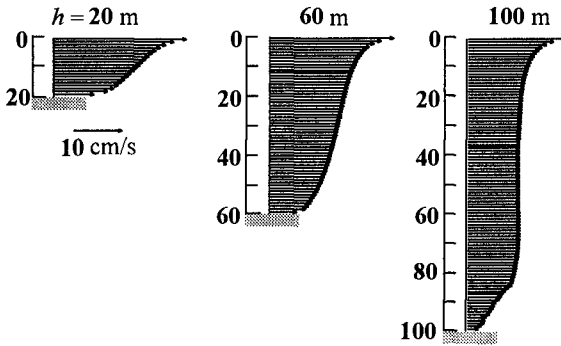


Fig.6 Computed vertical profiles of shore parallel velocity.

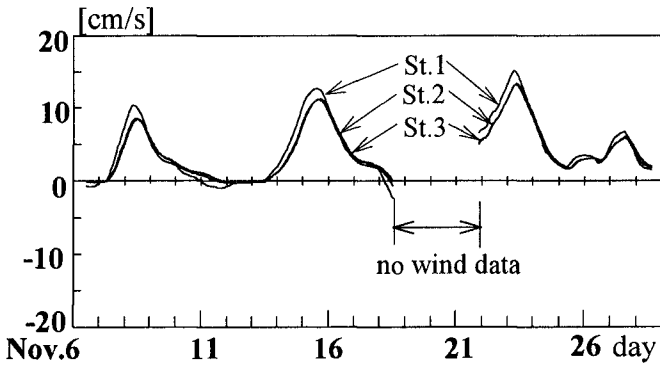


Fig.7 Computed shore-parallel velocities at St.1 to 3.

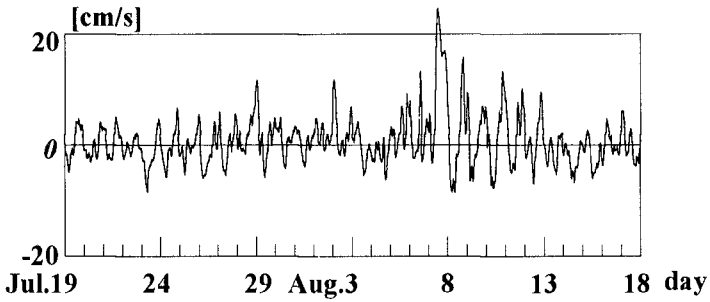


Fig.8(a) Shore-parallel component of bottom velocity at St.2.

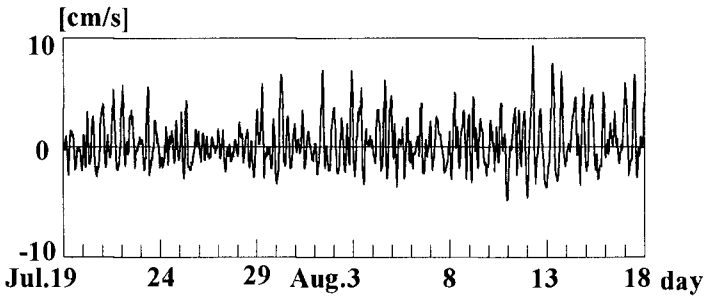
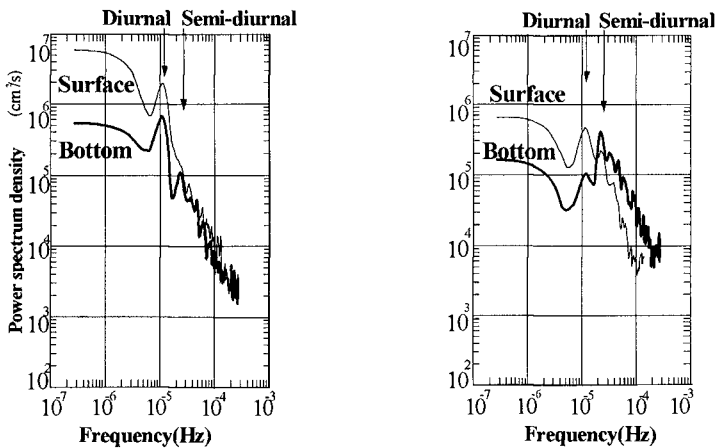


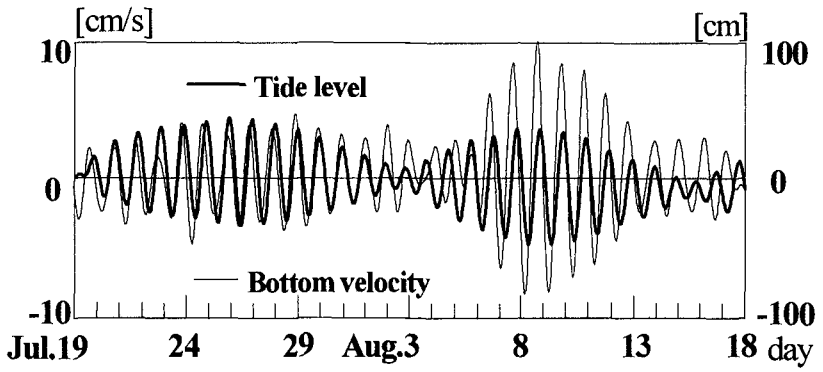
Fig.8(b) Cross-shore component of bottom velocity at St.2.



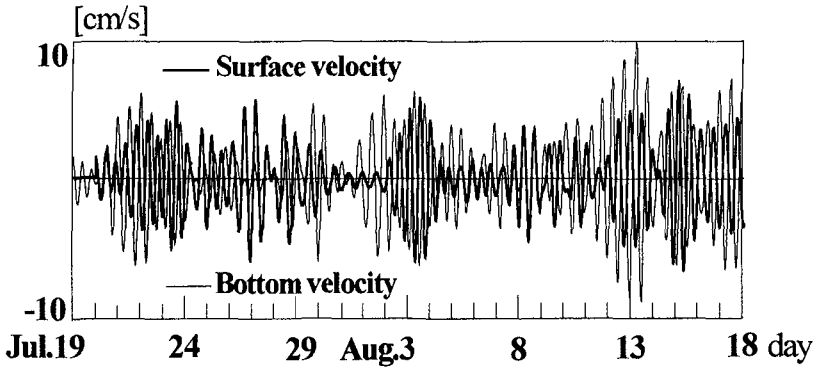
(a) Shore-parallel component.

(b) Cross-shore component.

Fig.9 Power spectra of velocity fluctuations at St.2.



(a) Diurnal component of shore-parallel bottom velocity and tide level at St.2.



(b) Semi-diurnal component of cross-shore bottom velocity and tide level at St.2.

Fig.10 Band-pass filtered velocities.

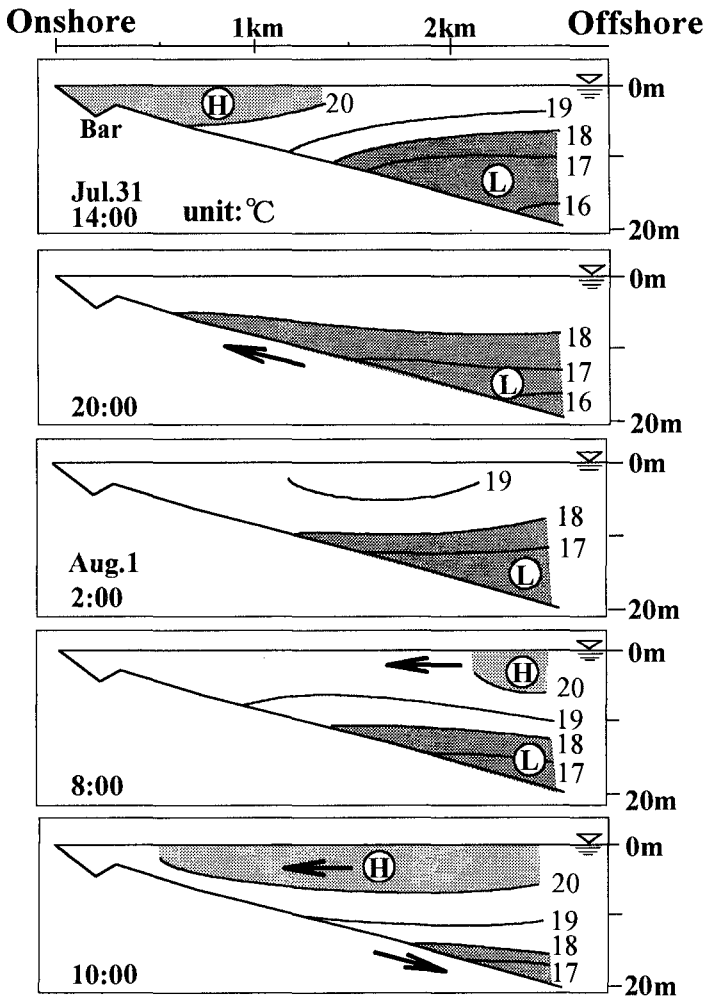


Fig. 11 Time sequence of spatial distribution of water temperature in diurnal time scale.